P H Y S I C A L   R E V I E W   L E T T E R S

Experimental Evidence for a Structural-Dynamical Transition in Trajectory Space

Rattachai Pinchaipat,[1,2] Matteo Campo,[3,4] Francesco Turci,[1,2] James E. Hallett,[1,2]
Thomas Speck,[4] and C. Patrick Royall[1,2,5,6]

[1]*H.H. Wills Physics Laboratory, Tyndall Avenue, Bristol BS8 1TL, United Kingdom*
[2]*Centre for Nanoscience and Quantum Information, Tyndall Avenue, Bristol BS8 1FD, United Kingdom*
[3]*Graduate School Materials Science in Mainz, Staudinger Weg 9, 55128 Mainz, Germany*
[4]*Institut für Physik, Johannes Gutenberg-Universität Mainz, Staudingerweg 7–9, 55128 Mainz, Germany*
[5]*School of Chemistry, University of Bristol, Cantock's Close, Bristol BS8 1TS, United Kingdom*
[6]*Department of Chemical Engineering, Kyoto University, Kyoto 615-8510, Japan*

Among the key insights into the glass transition has been the identification of a nonequilibrium phase transition in *trajectory space* which reveals phase coexistence between the normal supercooled liquid (active phase) and a glassy state (inactive phase). Here, we present evidence that such a transition occurs in experiments. In colloidal hard spheres, we find a non-Gaussian distribution of trajectories leaning towards those rich in locally favored structures (LFSs), associated with the emergence of slow dynamics. This we interpret as evidence for a nonequilibrium transition to an inactive LFS-rich phase. Reweighting trajectories reveals a first-order phase transition in trajectory space between a normal liquid and a LFS-rich phase. We also find evidence for a purely dynamical transition in trajectory space.

Introduction.—The glass transition is one of the long-standing challenges in condensed matter. In particular, one seeks to understand how solidity emerges with little apparent change in structure [1]. A central aspect for the understanding of supercooled liquids is dynamic heterogeneity: on suitable observation time scales, local regions appear liquidlike (*active*) or solidlike (*inactive*) [2], suggesting that any successful explanation must include this phenomenon. A variety of theories have been proposed; indeed, whether the glass transition has a thermodynamic (implying structural) or dynamical origin remains unclear [1]. The former may relate to a transition to an *ideal glass* state at finite temperature with minimal configurational entropy and has recently received some support from numerical and theoretical work [3–5].

The dynamical interpretation posits that the glass transition is a dynamical phenomenon where local relaxation events in the form of active regions couple to one another [6]. This *dynamic facilitation* approach employs the language of phase transitions in order to explain the emergence of solidity, but with a key departure from equilibrium thermodynamics: here, the phase transitions occur in *trajectory space* [7–9] instead of configurational space. In such transitions, trajectories of small systems, with a duration of a few structural relaxation times, exhibit a transition between active and inactive states under a biasing field, which in simulation is compatible with the scaling expected for a first-order transition [8,10]. It is suggested that the dynamical heterogeneity exhibited by glass-forming liquids is the hallmark of such a dynamical phase transition [6].

An extension of this trajectory space approach concerns structural-dynamical transitions, which may provide a link between the thermodynamic (structure-based) and dynamical transition approaches [11,12]. Here, one exploits the fact that, while changes in structure upon supercooling in liquids are not dramatic, nor are they absent [13]. In fact, they contribute to the emergence of strongly heterogeneous dynamical states. For example, for a variety of model glass formers, geometric motifs known as locally favored structures (LFSs) associated with slow dynamics have been identified [14].

This suggests that the dynamical phase transition in trajectory space may have a structural element, with the inactive phase having exceptionally high concentrations of LFSs with respect to the active phase. This has been shown to be the case [11]. Moreover, selecting trajectories rich in LFSs (rather than being dynamically inactive) leads to a similar nonequilibrium phase transition between a glassy LFS-rich phase and the normal (LFS-poor) supercooled liquid. This transition was found by biasing the population of LFSs along the length of a trajectory. The effect of the bias amounts to a dynamical chemical potential for the time-averaged LFS population favoring the sampling of trajectories that are rich or poor in structure. To realize the nonequilibrium transition, in practice a field termed μ is applied which uses a Boltzmann weight to sample trajectories based on their time-averaged LFS population. This demonstrates coupling between structure and dynamics.

Now, to date, dynamical transitions have been carried out under such biasing fields, which are, of course, absent in experiments. However, even in equilibrium, evidence of such transitions can be found by considering the so-called large deviations of dynamical observables, which serve as order parameters for the transition [15]. Quantities such as

the mobility [8] and the time-integrated population of LFSs [11] exhibit non-Gaussian probability distributions with enhanced tails corresponding to exceptionally large (or small) values of the observable. Nonconvexity of these distributions indicates a nonequilibrium phase transition which is revealed by reweighting these distributions (equivalent to applying the dynamical chemical potential) in the form of two coexisting peaks in the distribution of the observable of interest averaged along the trajectory. In experiments at equilibrium, a correct sampling of the non-Gaussian tails thus indicates the transition.

Particle-resolved studies of colloids [16] provide data similar to that of a computer simulation, and they have been used to show structural change approaching dynamical arrest [17–19] and that shear banding may be interpreted as a nonequilibrium transition [20]. Moreover, simulation data show behavior consistent with dynamical facilitation [21]. Our aim here is to seek an *experimental* signature of the dynamical phase transitions in time-averaged LFS populations and mobility, which we confirm with computer simulations. To do this, we apply the μ field as postprocessing to the experimentally determined non-Gaussian distributions. We back up our results with simulations in two ways. First, we employ biased sampling using small systems similar to that used in Ref. [11]. We then use larger, unbiased simulations which we *subsample* to obtain trajectories corresponding to a small system, and we show that the transition is accessible to experiments.

Experiment.—We used poly(methyl methacrylate) colloids fluorescently labeled with a mean diameter of $\sigma = 1.99\ \mu\text{m}$ and a polydispersity of 8%. The particles were suspended in a density matched solvent to which salt was added to screen electrostatic interactions. We use confocal microscopy to track the particle coordinates [22]. Because of particle tracking limitations, errors are introduced in the coordinate data [23,24]. To determine the impact of the errors, we compared our experiment with a simulation, as shown in Fig. 1(b). Here, we see that applying a Gaussian distributed error with the standard deviation 0.05σ to the simulation data leads to results comparable to the experiment. Further details may be found in the Supplemental Material (SM) [25].

Simulation and analysis.—We employ the DYNAMO event driven molecular dynamics package [33]. We consider a hard sphere system of five equimolar species of identical mass and different diameters: {0.888, 0.9573, 1.0, 1.043, 1.112}. This system also has a polydispersity of 8%. We fix the system size at $N = 10\,976$. Time scales are scaled to the Brownian time of the experimental system. Further details can be found in the literature [14,34]. For the biased simulations, we follow the methods used previously [8,10,11], with $N = 125$ at $\phi = 0.56$. The trajectory length t_{obs} is chosen to be significantly greater than the relaxation time $t_{\text{obs}} = 200 \simeq 10\tau_\alpha$. Further details are discussed below and in the SM [25].
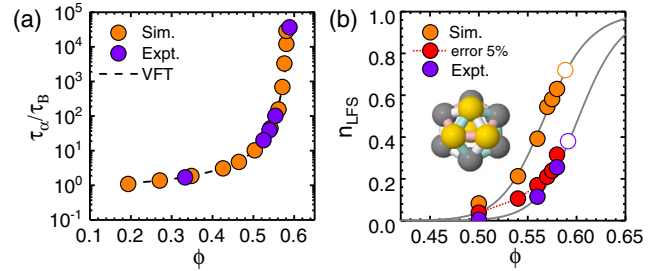
FIG. 1. Dynamical behavior and structural changes upon supercooling hard spheres. (a) Angell plot of structural relaxation time τ_α as a function of the volume fraction. The dashed line is the VFT fit described in the text. (b) The fraction of particles identified in defective icosahedra locally favored structures n_{LFS} increases upon supercooling. The simulation data with errors added to the coordinates (the red symbols) show quantitative agreement with the experiment. Unfilled symbols indicate a volume fraction corresponding to the LFS population in a LFS-rich phase. The grey lines are fits to $n_{\text{LFS}}(\phi)$ (see the SM [25]).

To analyze the local structure, we identify the bond network using the Voronoi construction with a maximum bond length of 1.4σ. We then use the topological cluster classification [35] (see the SM [25]) to identify the locally favored structure for the hard spheres, the ten-membered defective icosahedron (an icosahedron missing three particles) with C_{3v} symmetry depicted in Fig. 1(b) [36].

To determine the structural relaxation time τ_α, we calculate the intermediate scattering function reading $F(t) = 1/N \langle \exp\{i\mathbf{k} \cdot [\mathbf{r}(t + t') - \mathbf{r}(t')]\}\rangle$, where $|\mathbf{k}| = 2\pi$ is a wave vector taken close to the peak of the static structure factor, $\mathbf{r}$ is the coordinate, and the angle brackets indicate the averaging over all particles. We do not discriminate between particles of different size here. The structural relaxation time is then obtained by fitting a stretched exponential $F(t) = c \exp[-(t/\tau_\alpha)^b]$, as shown for the experimental data in the SM [25]. We compared experimental results with simulation through the Angell plot [Fig. 1(a)] to obtain the effective volume fraction.

Overall system behavior.—In Fig. 1(a), we show the dynamical behavior of the system, where we plot the structural relaxation time against the effective volume fraction for both experiments and simulations. Intermediate scattering functions are given in the SM [25]. We see that both experiments and simulations are well described by a Vogel-Fulcher-Tammann (VFT) fit $\tau_\alpha \propto \exp[A/(\phi_0 - \phi)]$, in which $\phi_0 = 0.606$ and $A = 0.24$ parametrizes the fragility as shown in Fig. 1(a), in line with previous work [14,37]. In Fig. 1(b), we see that, upon increasing ϕ, the population of locally favored structures [14] increases in both the experiments and the simulation. Once the errors in coordinate tracking in the experiments are accounted for, we find quantitative agreement with the simulation.

Evidence for a structural-dynamical phase transition.—Thus far, we have shown that the experimental hard sphere
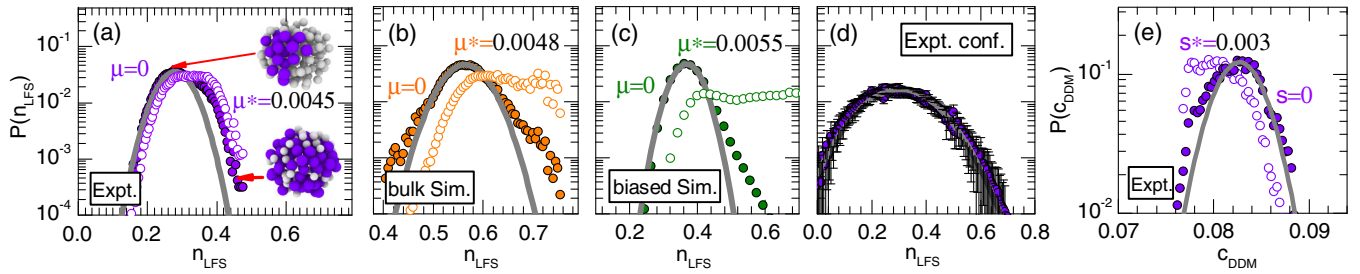
FIG. 2.   Probability distributions of populations (the filled symbols) of defective icosahedra in trajectories for the three systems we consider. Also shown is the postprocessed, reweighted data (the open symbols) demonstrating coexistence between normal liquid and LFS-rich phases in each case. (a) Experiment. Subsampled, volume fraction $\phi = 0.58$, trajectory length $t_{\mathrm{obs}} = 0.97\tau_\alpha$. Postprocessed data with $\mu^* = 0.0045$. (b) Bulk simulation data for $N_{\mathrm{tot}} = 10960$ particles. Subsampled, volume fraction $\phi = 0.575$, $t_{\mathrm{obs}} = 5\tau_\alpha$. Postprocessed data with $\mu^* = 0.0048$. (c) Biased simulation data for $N = 125$ particles. Full system with periodic boundaries, $\phi = 0.56$, $t_{\mathrm{obs}} = 10\tau_\alpha$. Postprocessed data with $\mu^* = 0.0055$. (d) Confirming the transition is dynamical. Experimental probability distribution of defective icosahedra obtained from *configurations* (rather than trajectories). (e) Experiment. DDM data to show dynamical transition subsampled, $\phi = 0.58$, $t_{\mathrm{obs}} = 1\tau_\alpha$. In all panels, grey lines indicate Gaussian distributions and thus reveal large deviations [and the absence thereof in (d)]. Except where indicated, the error bars are smaller than the symbols.

system undergoes structural change approaching dynamical arrest similar to the simulations [14]. Our strategy to provide evidence for a dynamical phase transition is as follows. First, we show that the hard sphere system undergoes the structural-dynamical phase transition previously identified in the binary Lennard-Jones system [11] in a small system of $N = 125$ particles. We then proceed to show that the same behavior, in the sense of a non-Gaussian probability distribution of the time-integrated fraction of particles in LFSs, n_{LFS}, is found in trajectories of $N = 100$ particles which have been *subsampled* from a bulk simulated system of $N_{\mathrm{tot}} = 10976$. This sets us up to perform a similar analysis on the experimental data. The larger than expected number of trajectories with a high population of LFSs is then evidence for a dynamical phase transition in the experimental system. We then apply a bias through the dynamical chemical potential μ by postprocessing unbiased simulated and experimental data to reveal coexisting populations of normal liquid and LFS-rich phases.

Biased simulations.—We compute the probability distribution for the population of LFSs along trajectories which are shown by the filled symbols in Fig. 2(c). Here, $\phi = 0.56$. We observe a peak at the equilibrium value $n_{\mathrm{LFS}} \simeq 0.37$, and a broad tail for high populations of LFSs that differs significantly from the Gaussian distribution expected for normal liquids which are not supercooled or supersaturated. To bias the system towards phase coexistence between the normal liquid and the LFS rich phase, we promote those high population trajectories by reweighting the $\mu = 0$ histogram:

$$P_\mu(n_{\mathrm{LFS}}) \propto P(n_{\mathrm{LFS}}) \exp[\mu n_{\mathrm{LFS}} N(K+1)], \qquad (1)$$

where $K + 1$ is the number of frames in the trajectories. From the double-peaked distribution in Fig. 2(c), we see that applying the μ field and increasing it above $\mu^* = 0.0055$ causes the system to undergo a transition from a low

population of LFSs ($n_{\mathrm{LFS}} \simeq 0.37$) to a high population ($n_{\mathrm{LFS}} > 0.7$). By reweighting with $\mu^* = 0.0055$, we see that the tail rises to the same height of the first peak, indicating that, at this value of μ, we have coexistence of the two phases in trajectory space. In other words, we have shown that hard spheres also exhibit the previously found dynamical phase transition [11].

Bulk simulations.—Having shown that the hard spheres undergo a structural-dynamical phase transition, we consider bulk simulations. Subsampled data for trajectories of $N = 100$ particles and length $5\tau_\alpha$ are shown in Fig. 2(b) for $\phi = 0.575$. We subsample the trajectories as shown schematically in Fig. 3. In simulation, the closest $N - 1$ particles to a given particle define the trajectory. We harvest trajectories of length $t_{\mathrm{obs}} = K\triangle t$, where $K + 1$ is the total configuration when using $n_{\mathrm{LFS}} = \mathcal{N}/[N(K+1)]$, $\mathcal{N}$ is the number of particles in the LFS, $\mathcal{N} = \sum_{k=0}^{N} \sum_{i=0}^{K} h_k^{(\mathrm{LFS})}(t_i)$. Here, $h_k^{(\mathrm{LFS})}(t_i) = 1$ if the particle is a member of a LFS and 0 otherwise. Further details are shown in the SM [25]. We see that the trajectory distribution is again non-Gaussian and find a shoulder corresponding to LFS-rich trajectories, like the unbiased data in Fig. 2(c) and that shown in Ref. [11].

Analyzing unbiased trajectory data.—The non-Gaussian behavior in Figs. 2(b) and 2(c) with its characteristic "fat
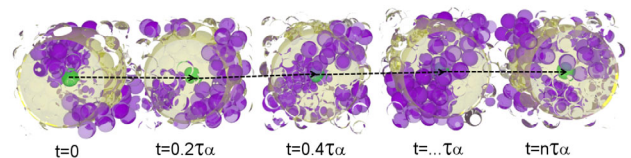
FIG. 3.   Illustration of the subsampling of trajectories. Purple particles are in defective icosahedra LFSs, while non-LFS particles are rendered transparent. In the experiments, we define the trajectories by considering the fraction of particles in LFSs in a sphere which contains ≈100 particles (the yellow tinted sphere). Here, $n\tau_\alpha$ is the length of the trajectory.

tail" demonstrates the dynamical phase transition. Here, we go further to reveal phase coexistence by reweighting the trajectory distributions. To do so, we apply the dynamical chemical potential μ via Eq. (1). We see in Fig. 2(b) that applying the μ field leads to a distribution indicating the same two coexisting phases, identified under the biased simulations in Fig. 2(b), one LFS rich and one LFS poor (the normal liquid). Crucially, because we have subsampled from a large, *unbiased* system, we demonstrate that it is possible to identify the nonequilibrium phase transition in experimental data, which is itself, of course, unbiased.

Nonequilibrium phase transition in experiments.—We now proceed to demonstrate the nonequilibrium transition in experiments. Our strategy follows that applied to the large unbiased simulations above. Specifically, we subsampled the tracked coordinates from the experiment for trajectories of length $0.97\tau_\alpha$. For the experiments, trajectories are defined by the evolution of the $N-1$ closest particles assigned *at the start* of the trajectory; see Fig. 3 and the SM [25]. In our case $R \approx 2.8\sigma$, which corresponds to ≈ 100 particles around a randomly chosen center particle.

In Fig. 2(a) we plot the LFS trajectory distributions. As before, we see the characteristic non-Gaussian distribution of trajectories, indicating a nonequilibrium phase transition. We see behavior similar to that of the simulations, in that there is a fat tail of LFS-rich trajectories, revealing the inactive phase. Because of the particle tracking errors, the distribution has a lower mean in Fig. 2(a); however, its relative width is comparable to that in Figs. 2(b) and 2(c).

Significantly, we expect (as shown previously in simulation [11]) that, when simply sampling configurations rather than *trajectories*, there should be a Gaussian distribution. That is to say, the phase transition has a dynamical character (rather than a conventional thermodynamic phase transition, which would be revealed by coordinate data only). This we find, as shown in Fig. 2(d). Thus, we provide evidence that the transition is trajectory based, i.e., that the dynamics are intrinsic to the transition, and thus it has a nonequilibrium nature. Another important check we need to make is that the transition is related to the particular LFS. In the SM [25], we show that trajectory sampling with a structure distinct from the LFS does not lead to a dynamical transition. Furthermore, we show that, by controlling the dynamical chemical potential μ, we can select either phase from the experimental data in Fig. 4. In this way it is possible, in an experiment, to identify configurations of the inactive phase.

In Fig. 1(b) (the unfilled symbols), we estimate the volume fraction that the LFS-rich phase corresponds to as 0.59. To do so, we determine the LFS population as a function of volume fraction $n_{\mathrm{LFS}}(\phi)$ (see the SM [25]), as indicated by the grey lines in Fig. 1(b). Under the VFT fit in Fig. 1(a), this corresponds to a structural relaxation time 300 times that of the system from which the trajectories are sampled, $\phi = 0.58$ for the experiments and some 1.8×10^4
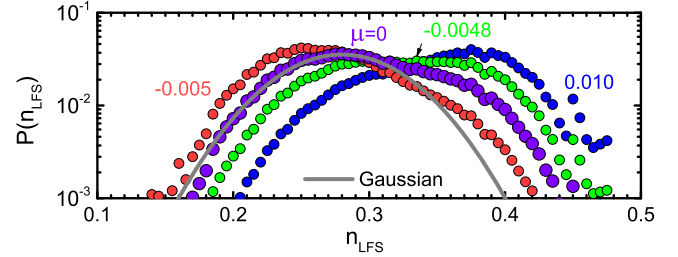
FIG. 4. Experimental probability distributions of LFS populations for several biases μ at volume fractions where $\phi = 0.58$.

in the case of the biased simulations, which are sampled at $\phi = 0.56$. In the future, with real-time data processing and using optical tweezers [38], it may even be possible to "freeze" such an inactive configuration and further probe its behavior—for example, by determining its rheological properties.

Finally, we consider the purely dynamical transition to a state of trajectories with very slow dynamics. This is shown in Fig. 2(e). Now the measurements of the displacements necessary are rather hampered by the particle tracking errors. We therefore determine the mobility with confocal differential dynamic microscopy (DDM) [39,40] as described in the SM [25]. We see that there is a fat tail for low mobility, indicating a dynamical transition. This is also found in the simulation, for which details are presented in the SM [25].

Conclusions.—We have demonstrated the existence of a dynamical phase transition in trajectory space *in experiments* between a normal liquid and a LFS-rich phase. This opens a perspective as to the range of dynamical phase transitions that might be identified by this kind of analysis. Here, we have focused mainly on structure (which is easier to identify in our experiments), but we have also demonstrated the purely dynamical phase transition. We have previously shown that there appears to be some overlap between the configuration space these transitions sample [11]. We see no reason to suppose that the current hard spheres should be significantly different. While some work has suggested that the hard sphere LFSs might have a hexagonal symmetry [41], no evidence of such order has been seen in a number of other studies, including this [34,36,42]. Finally, we find that trajectory biasing based on LFSs can produce configurations of exceptionally low configurational entropy, suggesting a link between LFSs and configurational entropy [12].

---

[1] L. Berthier and G. Biroli, Rev. Mod. Phys. **83**, 587 (2011).
[2] D. N. Perera and P. Harrowell, Phys. Rev. E **54**, 1652 (1996).
[3] C. Cammarota and G. Biroli, Proc. Natl. Acad. Sci. U.S.A. **109**, 8850 (2012).
[4] W. Kob and L. Berthier, Phys. Rev. Lett. **110**, 245702 (2013).
[5] M. Ozawa, W. Kob, A. Ikeda, and K. Miyazaki, Proc. Natl. Acad. Sci. U.S.A. **112**, 6914 (2015).
[6] D. Chandler and J. P. Garrahan, Annu. Rev. Phys. Chem. **61**, 191 (2010).
[7] R. L. Jack, M. F. Hagan, and D. Chandler, Phys. Rev. E **76**, 021119 (2007).
[8] L. O. Hedges, R. L. Jack, J. P. Garrahan, and D. Chandler, Science **323**, 1309 (2009).
[9] I. Thompson, Ph.D. thesis, University of Bath, 2015, http://opus.bath.ac.uk/46139/.
[10] T. Speck and D. Chandler, J. Chem. Phys. **136**, 184509 (2012).
[11] T. Speck, A. Malins, and C. P. Royall, Phys. Rev. Lett. **109**, 195703 (2012).
[12] F. Turci, C. P. Royall, and T. Speck, arXiv:1603.06892 [Phys. Rev. X (to be published)].
[13] C. P. Royall and S. R. Williams, Phys. Rep. **560**, 1 (2015).
[14] C. P. Royall, A. Malins, A. J. Dunleavy, and R. Pinney, J. Non-Cryst. Solids **407**, 34 (2015).
[15] H. Touchette, Phys. Rep. **478**, 1 (2009).
[16] A. Ivlev, H. Loewen, G. E. Morfill, and C. P. Royall, *Complex Plasmas and Colloidal Dispersions: Particle-Resolved Studies of Classical Liquids and Solids* (World Scientific Publishing, Singapore, 2012).
[17] M. Leocmach and H. Tanaka, Nat. Commun. **3**, 974 (2012).
[18] S. Mazoyer, F. Ebert, G. Maret, and P. Keim, Eur. Phys. J. E **34**, 101 (2011).
[19] C. P. Royall, S. R. Williams, T. Ohtsuka, and H. Tanaka, Nat. Mater. **7**, 556 (2008).
[20] V. Chikkadi, D. M. Miedema, M. T. Dang, B. Nienhuis, and P. Schall, Phys. Rev. Lett. **113**, 208301 (2014).
[21] M. Isobe, A. S. Keys, D. Chandler, and J. P. Garrahan, Phys. Rev. Lett. **117**, 145701 (2016).
[22] M. Leocmach, http://dx.doi.org/10.5281/zenodo.31286 (2015).
[23] C. P. Royall, W. C. K. Poon, and E. R. Weeks, Soft Matter **9**, 17 (2013).
[24] C. P. Royall, A. A. Louis, and H. Tanaka, J. Chem. Phys. **127**, 044507 (2007).
[25] See Supplemental Material at http://link.aps.org/supplemental/10.1103/PhysRevLett.119.028004, which includes Refs. [26–32], for supporting data and description of experimental and computational methods.
[26] M. Leocmach and H. Tanaka, Soft Matter **9**, 1447 (2013).
[27] C. P. Royall and W. Kob, J. Stat. Mech. (2017) 024001.
[28] W. C. K. Poon, E. R. Weeks, and C. P. Royall, Soft Matter **8**, 21 (2012).
[29] L. Berthier and R. Jack, Phys. Rev. E **76**, 041509 (2007).
[30] A. L. Thorneywork, R. E. Rozas, R. P. A. Dullens, and J. Horbach, Phys. Rev. Lett. **115**, 268301 (2015).
[31] P. G. Bolhuis, D. Chandler, C. Dellago, and P. L. Geissler, Annu. Rev. Phys. Chem. **53**, 291 (2002).
[32] D. D. L. Minh and J. D. Chodera, J. Chem. Phys. **131**, 134110 (2009).
[33] M. N. Bannerman, R. Sargant, and L. Lue, J. Comput. Chem. **32**, 3329 (2011).
[34] C. P. Royall, S. R. Williams, and H. Tanaka, arXiv:1409.5469.
[35] A. Malins, S. R. Williams, J. Eggers, and C. P. Royall, J. Chem. Phys. **139**, 234506 (2013).
[36] C. P. Royall, A. Malins, A. J. Dunleavy, and R. Pinney, J. Non-Cryst. Solids **407**, 34 (2015).
[37] G. Brambilla, D. El Masri, M. Pierno, L. Berthier, L. Cipelletti, G. Petekidis, and A. B. Schofield, Phys. Rev. Lett. **102**, 085703 (2009).
[38] I. Williams, E. C. Oğuz, T. Speck, P. Bartlett, H. Löwen, and C. P. Royall, Nat. Phys. **12**, 98 (2016).
[39] P. J. Lu, F. Giavazzi, T. E. Angelini, E. Zaccarelli, F. Jargstorff, A. B. Schofield, J. N. Wilking, M. B. Romanowsky, D. A. Weitz, and R. Cerbino, Phys. Rev. Lett. **108**, 218103 (2012).
[40] R. Cerbino and V. Trappe, Phys. Rev. Lett. **100**, 188102 (2008).
[41] H. Tanaka, T. Kawasaki, H. Shintani, and K. Watanabe, Nat. Mater. **9**, 324 (2010).
[42] B. Charbonneau, P. Charbonneau, and G. Tarjus, Phys. Rev. Lett. **108**, 035701 (2012).